Introduction

Full waveform inversion (FWI) is a challenging data-fitting technique, based on full wavefield propagation and a nonlinear inversion algorithm, to obtain an accurate model of underground media. With the advance of high performance computing and multi-component wide-aperture and wide-azimuth acquisitions, full waveform inversion has become increasingly powerful for extracting reliable subsurface information.

Lailly (1983) and Tarantola (1984) developed the original idea of gradient-based full waveform inversion. It can be implemented in either the frequency domain (Tarantola, 1984; Mora,1987) or the time domain (Pratt, 1990; Pratt and Worthington,1990). Recent research has been focused on reducing the intensive computation of FWI. Sirgure and Pratt (2004) selected limited frequencies for FWI. Shin (2006), and Bunks (1995), use a logarithmic domain and multiple grids in the time domain respectively. Denes and Starr (2008) use 3D prestack plane-wave reverse time migration to improve the computational efficiency. Nowadays, FWI algorithms have been verified by 2D/3D synthetic data and also have been applied to real data (Thierry, 1999a, 1999b, Operto, 2003, 2004).

In order to obtain a velocity model at deeper zones with high solution and accuracy, we require larger offsets and a higher domain frequency (Sirgue, 2004; Mulder, 2008; Operto, 2009). However, for surface acquisition, the maximum offset and domain frequency are limited. The domain frequencies of vertical seismic profile (VSP) data and cross-well data are much higher than that of surface seismic data. Moreover, the borehole-receiver acquisitions straightforwardly record seismic wavefield at greater depth. Therefore, a joint full waveform inversion of surface seismic data, VSP and cross-well data is proposed in this paper to improve the resolution of FWI.

Methods

Forward problem in space-frequency domain

In the space-frequency domain, the wave equation can be reduced as a linear system (Marfurt, 1984):

$$\mathbf{B}(\mathbf{x},\omega)\mathbf{u}(\mathbf{x},\omega) = \mathbf{s}(\mathbf{x},\omega) \tag{1}$$

where **B** is the impedance matrix; **u** is the seismic wavefield of pressure and **s** is the source term. Equation 1 can be solved by the LU decomposition of B, which makes the calculation more efficient and parallelizable (Stekl and Pratt, 1998; Hustedt et al., 2004).

Gauss-Newton Inversion

The aim of full waveform inversion is to obtain an accurate model of underground media. We seek the model **m** which minimizes the differences at receiver positions between observed seismograms $\mathbf{d}_{\text{obs}}$ and synthetic seismograms $\mathbf{d}_{\text{cal}}(\mathbf{m})$. Thus we define the misfit vector $\Delta\mathrm{d}(\mathrm{m}) = \mathrm{d}_{\text{obs}} - \mathrm{d}_{\text{cal}}(\mathrm{m})$. The misfit function (least-squares norm) is given by

$$\mathrm{E}(\mathbf{m}) = \frac{1}{2}\Delta\mathbf{d}^{\dagger}\Delta\mathbf{d} \tag{2}$$

where † indicates the transpose conjugate. The aim of FWI is to find a model m to minimize the least-squares norm by iteration. To speed up convergence, a Gauss-Newton method (Pratt et al., 1998) can be used as follows,

$$\delta\mathbf{m} = -(\mathbf{H}_{\mathrm{a}} + \lambda\mathbf{I})^{-1}\nabla_{\mathbf{m}}\mathrm{E}(\mathrm{m}) \tag{3}$$

where $\mathrm{H}_{\mathrm{a}} = \mathcal{R}e\{\mathrm{J}^{\mathrm{t}}\mathrm{J}^{*}\}$ represents the approximate Hessian matrix, J is the Jacobian matrix (Fréchet derivative matrix); λ is a damping factor to avoid singular values.

Strategy for efficient multi-scale inversion

Multi-scale inversion consists of two different levels: multi-grid and multi-frequency. Firstly, for the large-scale inversion problem, it is computationally inefficient to use fine grids on the whole model. This multi-grid method (Press and Teukolsky, 1991; Bunks et al., 1995) is to get the general coarse model by large grids, and then to fine up the interesting area by successively shorter scales. This method not only improves computational efficiency but also avoids the iteration results falling into the local minimum (Bunks et al., 1995).

Secondly, on each scale of multi-grid inversion, we use the multi-frequency strategy proposed by Sirgue and Pratt (2004) for optimizing the frequency interval of FWI, in order to ensure continuous wavenumber coverage of the recovered model without aliasing. The idea of this strategy is to reconstruct a wider band of wavenumbers using the signal at certain frequencies from far offset instead of that in a set of frequencies from near offset. The larger the maximum offset is, the fewer frequencies are needed. The formula for choosing frequencies is derived from a 1D velocity model by Sirgue and Pratt (2004) as follows:

$$f_{n+1} = \frac{f_n}{\propto_{min}} \tag{4}$$

where f_n is the frequency of the current iteration and f_{n+1} is the frequency to be chosen for the next iteration; $\propto_{min} = 1/\sqrt{1+r^2}$ is the parameter related to the ratio r of half-offset and maximum depth to be recovered.

Synthetic data test

In this paper, we use a Marmousi model to test the joint inversion method. Four acquisition geometries are designed as shown in Fig.1. The first three acquisitions are surface seismic acquisition (Fig.1(c)), VSP (Fig.1(d)) and cross-well seismic acquisition (Fig.1(g),(h)) respectively. The last one (Fig.1(e),(f)) is a combination of the first two acquisitions. The synthetic seismograms are modelled using a Ricker wavelet with 25Hz domain frequency. The bandwidth is around 0-62Hz. For the inversion problem, we choose a series of frequencies ranged from 3.0Hz to 20Hz for surface seismic inversion (Fig.1(c)) and joint inversion (Fig.1(e)) according to Sirgue and Pratt's (2004) theory, and from 3.0Hz to 50Hz for VSP (Fig.1(d)), cross-well inversion (Fig.1(g),(h)) and joint inversion (Fig.1(f)).

The inversion results and accuracy analysis are shown in Fig.1 and Fig.2 separately. Surface seismic FWI provides an acceptable result in the middle and shallow zones of the Marmousi model. However, in the area close to the model's edges, the resolution of the inversion result is low because of the lack of information for far offsets. VSP FWI can improve the accuracy of the model only around the borehole receivers, even for the greater depth of the model (Figs.2(a),(b),(c)). The joint inversion of surface seismic data and VSP seismic data promises a better result than the former two. Moreover, for the most interesting zones, we resort to cross-well data FWI for further improving the resolution, as shown in Figs.1(g) and (h). From the red line in Figs.2(d),(e) and (f), we can conclude that cross-well data inversion lead to the best resolution among those acquisition geometries discussed in this paper. It is also shown in the inversion results for multi-scale inversion (Fig.3) that the resolution is improved gradually with the wider bandwidth and finer grids.

Discussions and conclusions

In this paper, we discuss the solutions of FWI using four kinds of acquisition geometry in a synthetic case study of a Marmousi model. A strategy of joint inversion is proposed for better resolution, where the frequency is intrinsically sequentially increasing for surface, VSP and cross-well seismic data. This joint inversion strategy could be implemented as an optimized multi-scale method, as well.

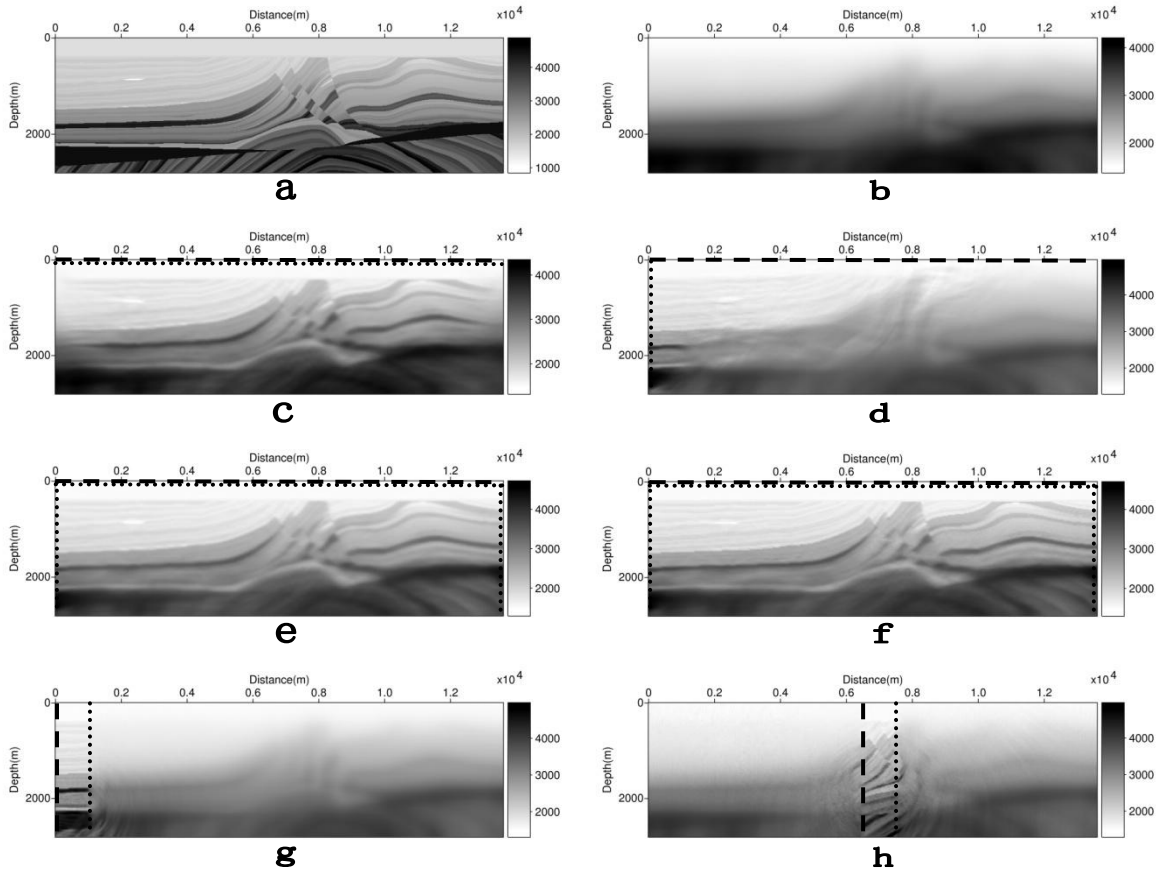

Figure 1 *True model, initial model and inversion results of a 2D Marmousi model using different acquisition geometries. The black dashed lines represent the location of sources while the dotted lines represent the location of receivers. (a) True Marmousi model. (b) Initial smoothed model. (c) Surface seismic FWI result. (d) VSP FWI result. (e) Joint inversion of surface seismic and VSP data from 3.0Hz to 20Hz. (f) Joint inversion of surface seismic and VSP data from 3.0Hz to 50Hz. (g) Cross-well seismic data inversion of the left part of the Marmousi model. (h) Cross-well seismic data inversion of the middle of the Marmousi model.*

References

Bunks, C., F. M. Saleck, et al. [1995]. Multiscale seismic waveform inversion. Geophysics 60(5): 1457-1473.

Lailly, P. [1983]. The seismic inverse problem as a sequence of before stack migrations, Society for industrial and applied mathematics.

Mora, P. [1987]. Nonlinear two-dimensional elastic inversion of multioffset seimic data. Geophysics 52(9): 18.

Mulder, W. A. and R. E. Plessix [2008]. Exploring some issues in acoustic full waveform inversion. Geophysics Prospecting 56: 1218-1228.

Operto, S., J. Virieux, et al. [2009]. Finite-difference frequency-domain modeling of viscoacoustic wave propagation in 2D tilted transversely isotropic (TTI) media." Geophysics 74(5): T75-T95.

Pratt, R. G. [1990]. Short Note: Frequency-domain elastic wave modeling by finite differences: A tool for crosshole seismic imaging. Geophysics 55(5): 626-632.

Pratt, R. G. and M. H. Worthington [1990]. Inverse theory applied to multi-source cross-hole tomography. Part 1: Acoustic wave-equation method. Geophysics Prospecting 38: 311-329.

Shin, C. and D.-J. Min [2006]. Waveform inversion using a logarithmic wavefield. Geophysics 71(3): R31-R42.

Sirgue, L. and R. G. Pratt [2004]. Efficient waveform inversion and imaging: A strategy for selecting temporal frequencies. Geophysics 69(1): 231-248.
Tarantola, A. [1987]. Inverse problem theory, Society for industrial and applied mathematics.
Virieux, J. and S. Operto [2009]. An overview of full-waveform inversion in exploration geophysics. Geophysics 74(6): WWC127-WWC152.

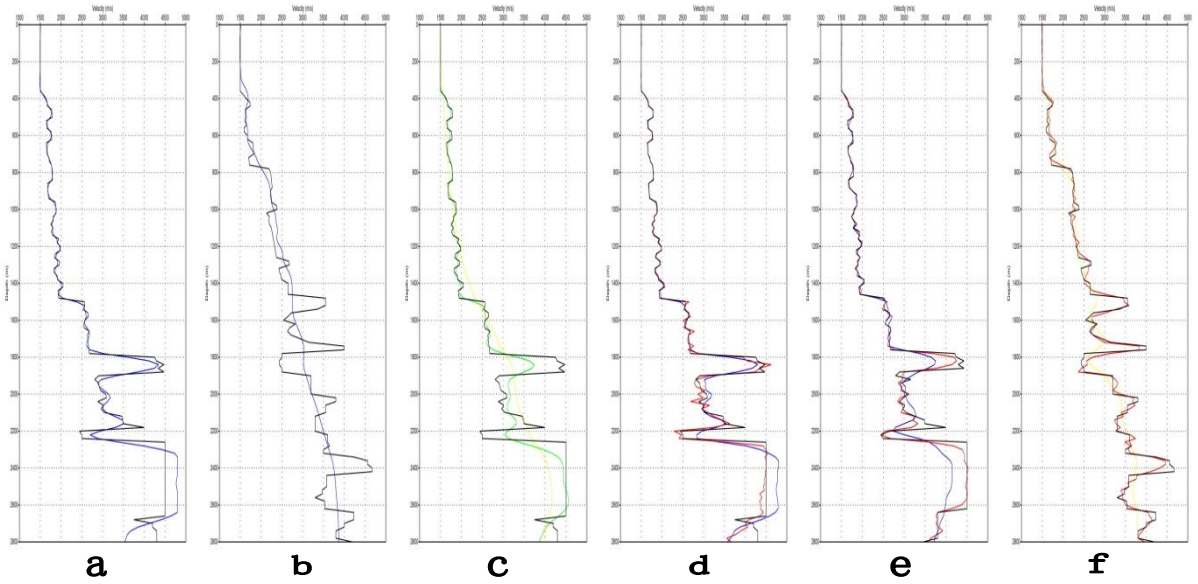

Figure 2 *Comparisons of the vertical velocity graphs extracted from the true model (black line) and inversion results (yellow for surface inversion, blue for VSP, green for joint inversion and red for cross-well). (a) and (b) Vertical velocity graphs of VSP inversion (Fig.1 (d)) at 0km and 7.0km distance respectively. (c) Vertical velocity graphs of surface seismic inversion (Fig.1 (c)) and joint inversion (Fig.1 (e)) at 0km distance. (d) Vertical velocity graphs of VSP inversion (Fig.1 (d)) and cross-well inversion (Fig.1 (g)) at 0km distance. (e) Vertical velocity graphs of VSP inversion (Fig.1 (d)) and cross-well inversion (Fig.1 (g)) at 1.0km distance. (f) Vertical velocity graphs of surface seismic inversion (Fig.1 (c)) and cross-well inversion (Fig.1 (h)) at 7.0km distance.*

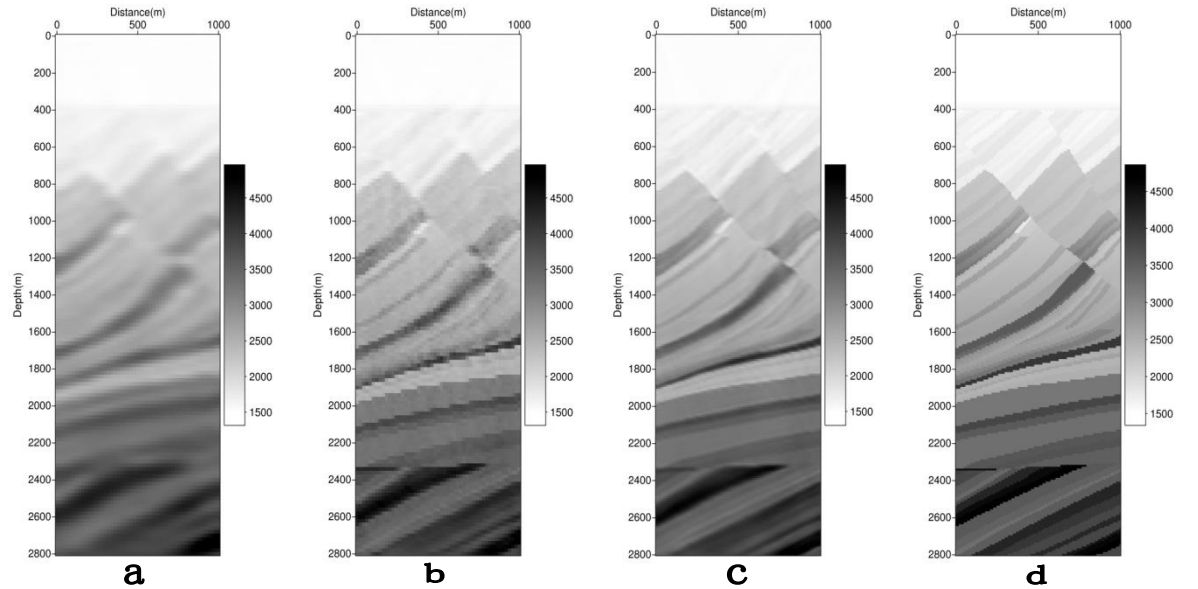

Figure 3 *Multi-scale inversion results on the target zone of the Marmousi model. (a) Inversion result using 20m-spaced grids and 0-20 bandwidth. (c) Inversion result using 20m-spaced grids and 0-50 bandwidth. (c) Inversion result using 10m-spaced grids and 0-50 bandwidth. (d) True velocity model*